Nano Research
2023, 16(9): 11871–11877

ISSN 1998-0124 CN 11-5974/O4
https://doi.org/10.1007/s12274-023-5623-0

Research Article

Low-frequency blue energy harvesting for sustainable and active anticorrosion

Miaomiao Cui[1,§], Yawei Feng[1,§], Hao Wu[1,3], Yuankai Jin[1], Wanbo Li[1,4], and Zuankai Wang[2] (✉)

[1] *Department of Mechanical Engineering, City University of Hong Kong, Hong Kong, China*
[2] *Department of Mechanical Engineering, The Hong Kong Polytechnic University, Hong Kong, China*
[3] *School of Physics and Optoelectronics, South China University of Technology, Guangzhou 510640, China*
[4] *Interdisciplinary Research Center for Engineering Science, School of Mechanical Engineering, Shanghai Jiao Tong University, Shanghai 200240, China*
[§] *Miaomiao Cui and Yawei Feng contributed equally to this work.*

Received: 31 January 2023 / **Revised:** 21 February 2023 / **Accepted:** 27 February 2023

ABSTRACT

Engineering materials serving in marine surroundings are inevitably corroded. The corrosive marine conditions can also be utilized to harvest kinetic ocean wave energy to solve this problem. Leveraging water–solid triboelectrification to harvest low-frequency wave energy for active anticorrosion is promising. Existing techniques are efficient in harnessing environmental energy with frequencies higher than 3 Hz, whereas the dominated ocean waves with optimal wave spectral density fluctuate from 0.45 to 1.5 Hz. Herein, we proposed a highly efficient and sustainable blue energy-powered cathodic protection (BECP) strategy by fusing water–solid triboelectric nanogenerators and cathodic protection technology. Leveraging the highly efficient triboelectrification between the moving water and hydrophobic fluorinated ethylene propylene tube, we developed the built-in power module, enabling the harvest of ocean wave energy lower than 1.5 Hz. The generated volumetric current density is 28.9 mA·m^{-3}, 5–20 times higher than the values of the reported devices. Moreover, the proposed BECP performs comparably to conventional cathodic protection in corrosion inhibition. Significantly, the proposed approach can be easily applied to ships, buoys, and other offshore platforms to simultaneously realize blue energy harvesting and engineering material protection, providing an alternative to traditional active protection technology.

KEYWORDS

corrosion inhibition, blue energy harvesting, triboelectric nanogenerator, cathodic protection

1 Introduction

The ocean is a complex world, containing diverse living organisms ranging from cellular scale to large mammalian scale, and crossing the temperate zone from 2 to 30 °C [1]. The complexity and variability of the marine conditions pose a plethora of technical challenges to the reasonable development and utilization of marine resources. One extraordinary challenge is the inevitable material corrosion caused by the interaction of metal structures with seawater or the wet atmosphere [2]. The undesired phenomena seriously threaten the service life of the applied engineering materials, generating material failure, economic loss, environmental damage, and even human death [3].

Various anticorrosion techniques, including passive and active manners, have been developed to suppress/delay materials destruction. Passive strategies such as incorporating inhibitors, anodic oxidation, and protective coatings have been extensively explored over the past decades [4–7], which isolate and kinetically protect substrate materials from the corrosive environment, presenting a passive and physical approach to combat the pressing corrosion issue [8, 9]. However, the passive strategies are unsustainable, for the surface layer of coating or inhibitor is irreversibly degraded and consumed under harsh circumstances. Even worse, the passive approaches always require organic substances that are harmful to the human body and environment. [10–13]. Compared with the passive protection methods, the active one is environmentally benign and protects materials from corrosion failure under any surroundings. Active protection methods, including the sacrificial anode approach and impressed current cathodic protection, offer the possibility to delay the failure of materials by controlling the thermodynamic factors of corrosion reactions. Nevertheless, active anticorrosion strategies rely on continuous metal consumption or electric power supply, which do not cater to sustainable and green development and challenge the application in widely distributed facilities.

Despite the complex environment, the ocean possesses massive wave energy, providing a vast potential to generate carbon-free and renewable electricity. Harnessing ocean wave energy to combat marine corrosion offers the possibility to eliminate the need for additional power in the active protection strategy. Recently, sustainable and active anticorrosion systems with built-in triboelectric nanogenerators (TENGs) have been developed [14–20]. TENGs were applied to convert ambient mechanical energy in the forms of wind blowing [21–27], fluid flowing [28–30], water waves [17, 19, 31–36], and water drops [37–43]

Address correspondence to zk.wang@polyu.edu.hk

into electricity, standing in contrast to the conventional power supply. Ocean wave, one typical mechanical wave, covers a wide range of frequencies (10^{-6}–10^{2} Hz) [44]. Particularly, the surface gravitational ocean waves centralized at 0.45 to 1.5 Hz govern the wave energy density spectra [45]. However, most TENG prototypes exhibit high performance in harvesting mechanical energy higher than 3 Hz [17–20], while less attention has been paid to harvesting ocean wave energy analogous to the real spectra. To fill the gap, developing a blue energy-powered cathodic protection (BECP) strategy to harness the low-frequency ocean wave energy is important.

In this work, we proposed a sustainable and active anticorrosion strategy by fusing electricity generation with cathodic protection. Electricity generation is based on triboelectric nanogenerators that are capable of harvesting low-frequency ocean wave energy to output high volumetric current density, which is 5–20 times higher than the existing technologies. Simultaneously, the generated electricity is provided to the metal substrate to resist material corrosion. By developing the BECP strategy, we successfully circumvent the inherent bottleneck imposed by the impressed current cathodic protection. Significantly, the BECP exhibits comparable performance as a cathodic protection system powered by commercial potentiostats and could protect a 1 cm^2 Q235 carbon steel surface free from corrosion. The BECP also imparts added-value benefits of efficient electricity generation and energy saving for corrosion resistance. The versatility, scalability, and portability of our system offer a disruptive technology and will find immediate applications in marine, such as on boats, passenger ships, large cargos, combat vessels, and other marine architectures.

2 Experimental

2.1 Materials

Acetone (RCI Labscan, 99.5%), sodium chloride (Traditional Chinese Medicine, analytically pure), ethanol (Sigma Aldrich, 97%), Teflon tape (Sterlitech Corporation, PTU023001), fluorinated ethylene propylene (FEP) tube, carbon tap, and copper tap were used without further purification. Q235 steel (27.6 wt.%, C 0.127 wt.%, Si 0.15 wt.%, Mn 0.41 wt.%, P 0.018 wt.%, S 0.019 wt.%, and Fe balance) with the size of 10 mm × 10 mm × 5 mm was employed as the metal substrate.

2.2 Fabrication and measurement of the triboelectric nanogenerator

FEP tube with a diameter of 1.2 cm was cut into sections with a length of 5.5 cm. The tube section was wrapped by two copper tapes (length of 2 cm) side by side and organized with the external circuit by the enameled conductive wire. After half a volume of water was filled, the tube was sealed with Teflon tapes. 54 units were assembled and placed into a Yagari box, ten of which were assembled together for a large-scale application, protecting the Q235 carbon steel. A commercial seesaw shaker was applied to simulate the generation of waves and to trigger the generator unit or array. All electrical properties were measured by Keithley 6514 system electrometer. The surface potential distribution upon the dielectric FEP surface was simulated by COMSOL Multiphysics in a two-dimensional mode. The tube model was set to be a rectangle according to the actual size: The length was 5.5 cm, the height was 1.24 cm, and the wall thickness was 0.02 cm. The original water volume was set to be half of the internal volume of the tube. Four copper electrodes (20 mm × 0.05 mm), including a grounded electrode and a floated electrode, were settled at a distance of 0.025 mm from the tube surface. The surface charge density on the internal wall of the tube was set to be −0.84 $\mu C \cdot m^{-2}$, while the value on the water surface was set to be 1.35 times (according to the surface area ratio) that of the tube surface. The mesh was constructed by the physical field-controlled sequence with the mesh size of the fine.

2.3 Immersion experiment

Q235 carbon steels were sealed by epoxy resin with a working surface of 1 cm^2 exposed and were polished with SiC papers from grade 400 to grade 1500. The smooth metal substrates were then ultrasonically cleaned with acetone and alcohol for 5 min, respectively. For the construction of the self-powered cathode protection system, a piece of carbon steel was connected to the negative pole of the rectifier (DB107), which was connected to the TENG array, and a platinum foil (2 cm^2) was connected to the positive pole of the rectifier. The generator array floated on a water bath and was motivated by the artificial water wave. The corrosion measurement was performed in the simulated seawater of 3.5 wt.% NaCl solution. Corrosion experiments involving any electricity and 5 V of direct current (DC) power protection were also conducted under the same conditions for comparison. The morphology of corroded carbon steel samples was captured by a camera at 4, 8, and 20 h immersion times, respectively.

2.4 Electrochemical measurements of corroded carbon steel

Electrochemical tests, including open-circuit potential (E_{OCP}) and polarization curves, were performed on an electrochemical workstation (CHI760E). The electrochemical experiments were carried out in the 3.5 wt.% NaCl aqueous solution. A three-electrode configuration was applied, including the metal sample, a platinum sheet, and a saturated calomel electrode (SCE) as working, counter, and reference electrodes, respectively. Potentiodynamic polarization curves (Tafel curves) were obtained by setting the sweeping range of ±300 mV versus the E_{OCP} value, and a rate of 1 $mV \cdot s^{-1}$ was employed for scanning. The Tafel curves were further fitted by Cview software to get the electrochemical parameters (self-corrosion current density (j_{corr})).

3 Results and discussion

Figure 1(a) shows the schematic drawing of the proposed BECP platform that consists of a wave energy harvester, conditional circuit, and self-corrosion cell. To harvest the low-frequency ocean wave energy, we designed a TENG array featuring with two sidewall copper electrodes dividing the triboelectric generator into two parts. To achieve high surface charge density and high output performance, the hydrophobic FEP with a high negative triboelectrification sequence was utilized as the tribo-material, and liquid water was encapsulated inside the FEP tube as the positive tribo-material. In response to the vibration, the encapsulated water takes close and dynamic interaction with the internal FEP tube, transforming the kinetic fluctuating wave energy into potential difference upon the two copper electrodes owing to the coupled triboelectrification and electrostatic induction [46–50]. Moreover, we applied a full-wave rectifier to convert the alternating current (AC) output from the generator array to DC to power the terminal cell for inhibiting the spontaneous corrosion of material in ocean conditions.

Converting ocean wave energy represents an excellent potential for renewable electricity generation. Most TENGs exhibit satisfying performance in harvesting mechanical energy higher than 3 Hz; however, the ocean waves possess a high spectral density in the vibrating frequency range of 0.45 to 1.5 Hz (Fig. 1(b)) [45], which is hard to be collected. After fabrication, we first

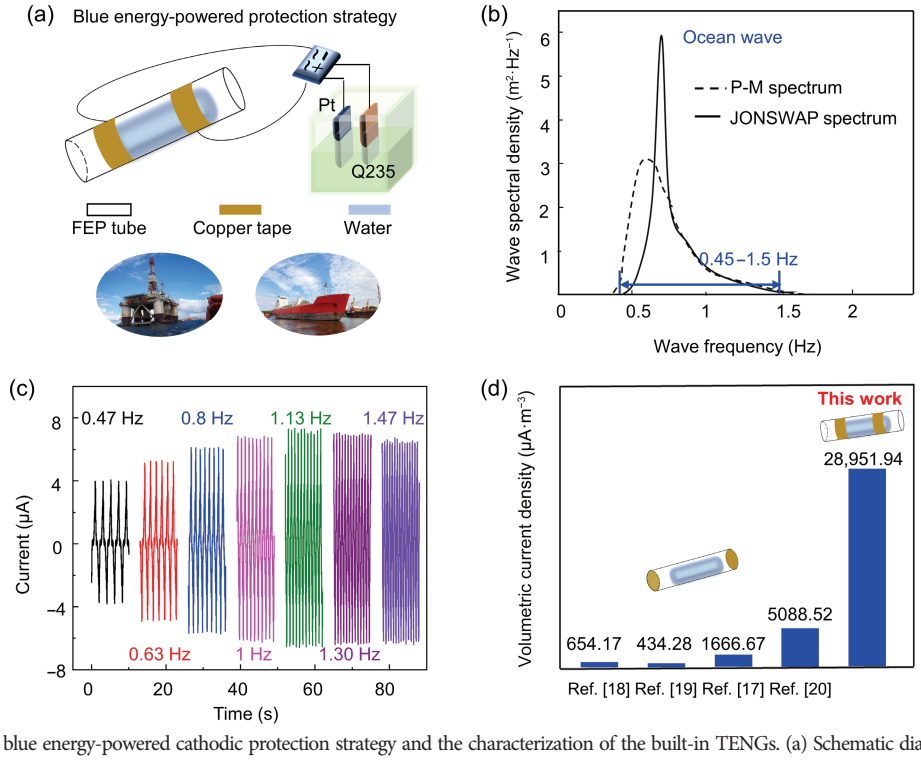

Figure 1 Design of the blue energy-powered cathodic protection strategy and the characterization of the built-in TENGs. (a) Schematic diagram of the blue energy-powered cathodic protection strategy. (b) The wave spectral density of ocean wave. (c) With an increase in the swinging frequency from 0.47 to 1.13 Hz, the output current from the TENG array increases gradually, followed by a slight decrease as the further increase of frequency (1.30 to 1.47 Hz). (d) The volumetric current density comparison of our work with the reported works under the excitation frequency of 1 Hz.

measured the short-circuit current (I_{SC}) from the TENG array under different triggering frequencies. The I_{SC} waveforms suggest the incremental intensity with the increased vibration frequency and reach the peak at 1.13 Hz. By contrast, we found that the previous competitors [17–20] have their peak output around 3 Hz. Due to the unsatisfactory resonance between the devices and ocean waves, the previous competitors exhibit disappointing performance in harvesting mechanical energy from ocean waves, whose vibrational frequency is generally less than 1.5 Hz. In addition, we calculated the volumetric current density, as shown in Fig. 1(d). It is demonstrated that the TENG is superior with a much higher volumetric current density (28,951.94 μA·m^{-3}), whose value is 5–20 times larger than the reported devices. The output performance is expected to be further enhanced by material surface engineering or a charge injection approach for a higher surface charge density [51].

The underlying reason for the supreme volumetric current density at low-frequency mechanical waves is the TENG configuration. The reported devices generally work well under high-frequency excitation (higher than 3 Hz) by facilitating electrodes on the two undersides of the water tube. In this condition, flowing water inside the FEP tube should be motivated to reach the electrodes to generate the induced electricity [19], resulting in unsatisfactory resonance between the devices and ocean waves. In contrast, we configured two copper electrodes at the sidewall of the cylindrical FEP tube. Under the same mechanical frequency of 1 Hz, we obtain a higher flowing current and the contributed output performance by effectively decreasing charge transfer time. What's more, we applied FEP exhibiting a more electro-negative sequence than other dielectric materials to obtain the increased surface charge density.

To illustrate the underlying mechanism for power generation, we inspected the interaction of the FEP surface and the water flow. Once the water flow contacts with the internal wall of FEP tube, the FEP with a more negative electrification serial would be negatively charged by extracting electrons from water. After the repeated motion of water fluids under the simulated waves, the surface of the internal FEP wall and water fluids are both charge-saturated for stable dielectric properties. At the horizontally placed stage (Fig. 2(a)(I)), the configuration of TENG is mirror symmetry; thus, each electrode is zero charged for the electrostatic balance. In this condition, the potential on each copper electrode is equal, as shown in Fig. 2(b)(I). As the fluctuation of simulated waves, water fluid moves from the left to the right side (Figs. 2(a)(I) and 2(a)(II)). Since the flowing water is positively charged, the original electrostatic balance is broken. Simultaneously, the polarization on the right side of the internal tube is net positive, and the polarization on the left side is net negative, which can also be visualized by the potential distribution in Fig. 2(b)(II). Under this condition, electrons should flow to the right from the left electrode to balance the excessive polarization. Therefore, a pulsed current from the right to the left electrode is formed along the external circuit for the electrostatic induction (Fig. 2(c)). After the water starts to retract back from the right side to the left side (Figs. 2(a)(II)–2(a)(IV)), the polarization upon each electrode reverses as illustrated in Figs. 2(b)(II)–2(b)(IV), leading to the backward flowing of electrons from right to left electrode along the external circuit. The periodic forward and backward water flowing triggered by the simulated waves contributes to the TENG's alternating output [17, 18, 20, 52]. Since we defined stage (I) as the initial stage, it shows a phase difference between the current waveform (Fig. 2(c)) and the transferred charge waveform (Fig. 2(d)).

In our device, the induced performance is determined by the water/FEP adhesion interface, which is affected by the flowing and spreading conditions of water fluid. The reduced water transfer period and the significant water–FEP contact area difference between the two parts FEP tube partitioned by copper electrodes are beneficial to the performance of TENG. Both parameters are frequency dependent, thus we explored the electric output under different mechanical frequencies. Under the static state (0 Hz), there is no output. As the vibration frequency increases from 0.47

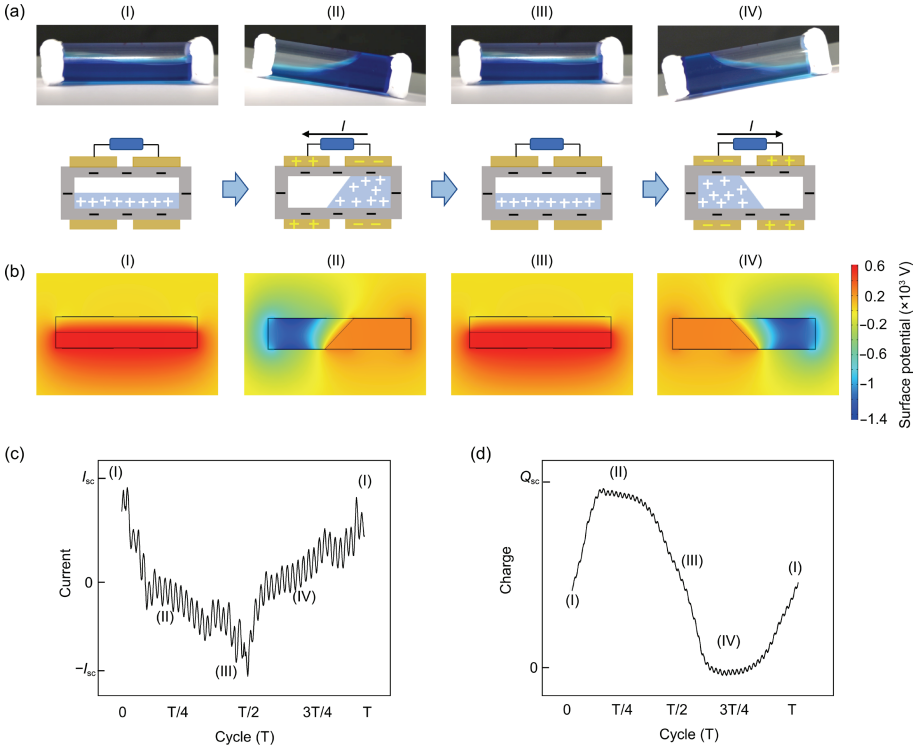

Figure 2 Synchronization of water-flow dynamics and electrical response. (a) Water-flow dynamics and the current flowing between FEP and water. (b) Finite element simulation of a periodic potential change. Time-dependent variations in (c) flowing current and (d) transferred charge from the TENG.

to 1.13 Hz, the maximum contact area difference increases for the rising acceleration (Fig. S1 in the Electronic Supplementary Material (ESM) and Video ESM1), and the water transfer period reduces. Therefore, the current is gradually increased, as plotted in Fig. S2(a) in the ESM. For all units synchronized in a unitive layout, our array gives a superimposed peak I_{SC} value of 7.4 μA at the frequency of 1.13 Hz. In addition, open-circuit voltage (V_{OC}) and transferred charge at short-circuit state (Q_{SC}) have the same trend due to the better liquid-phase response (Figs. S2(b)–S2(d) in the ESM), exhibiting the peak V_{OC} value of 80.05 V and Q_{SC} of 1.24 μC. Since the further increase of trigger frequency does not benefit the promoted water–FEP contact area difference, the output performance of TENG does not improve further. With the gradual increase of frequency from 1.13 to 1.47 Hz, water fluid is hard to transport from one side to the other for water inertia, rendering a slight decrease in the peak value.

Compared with the commercial power, the built-in TENG array exhibits renewable and sustainable electricity-generation performance that enables the proposed strategy to have potential superiority in protecting the scattered metal structures (Fig. 3(a)). Here, we explored the anticorrosion performance of the BECP by characterizing the electrochemical properties of vulnerable steel in simulated marine conditions. The Nyquist plots in Fig. S3(a) in the ESM exhibit that the radians of the curves decrease with the faster electron injection from the TENG array, indicating the accelerated charge transfer at stainless steel and solution interface. The charge transfer process is further verified by the lower charge transfer resistance (R_{ct}) at the carbon steel interface, as shown in the Bode plots (Fig. 3(b)). The lower R_{ct} also means that the metal surface is less likely to undergo oxidative corrosion for the accumulation of negative electrons in the cathodic protection system. Besides, the electrochemical process of Q235 carbon steel is fitted to the equivalent electronic circuit, as shown in Fig. S3(b) in the ESM. The fitted R_{ct} values decrease markedly from 1285.545 to 205.06 Ω·cm^{-2} when the vibrating frequency increases from 0.47 to 1.13 Hz (Fig. S3(c) in the ESM), suggesting better performance under more vigorous wave agitation. Significantly, the protection performance under 0.8 Hz by the constructed system is almost consistent with the contribution of a 5 V commercial potentiostat (Fig. 3(b)).

The electrochemical state of the Q235 plate was determined by probing the E_{OCP}. Under marine conditions, the bared Q235 carbon steel switches to an under-protection state from the self-corrosion state in the potential range of −0.926 to −1.226 V vs. SCE [52]. Once immersed in the corrosive solution, the bared Q235 carbon steel exhibits its E_{OCP} of −0.560 V vs. SCE (Fig. 3(c) and Fig. S3(d) in the ESM). After being impressed with negative electrons by the TENG array, the metallic plate underwent a sharp decrease in E_{OCP} that was finally stabilized at −1.1 V vs. SCE (Fig. S3(d) in the ESM), indicating that the Q235 plate was transferred to an under-protection state from the self-corrosion state. The periodic rise and drop of E_{OCP} value by the intermittent switch on and off the TENG array corresponds to the conclusion of the feasibility of cathodic protection. In addition, the plate revealed a more negative E_{OCP} shift when it was impressed with the TENG array under a higher wave vibrating frequency (Fig. S3(e) in the ESM). Specifically, the bared Q235 exhibits much negative E_{OCP} of −1.129 V vs. SCE at the vibration frequency of 1.0 Hz, while it negatively shifts to −1.141 V vs. SCE at the operation frequency of 1.13 Hz. More negative E_{OCP} of metal material is prone to be in a protected state; thus, our marine energy-powered cathodic protection system has excellent protection performance under the motivation of ocean waves. The similar E_{OCP} curve under the power of a 5 V commercial potentiostat also demonstrates the effectiveness of the proposed cathodic protection system.

The Tafel plots shown in Fig. 3(d) and Fig. S3(f) in the ESM not only exhibit the frequency-dependent corrosion potential variation but also render the self-corrosion current density. With the vibrating frequency increased to 1.13 Hz, fitted self-corrosion potential (E_{corr}) and j_{corr} remarkably drop from −0.68 to −1.1249 V and from 2.472 × 10^{-3} to 1.89 × 10^{-6} A·mm^{-2}, respectively (Fig. S3(c) in the ESM). The above results demonstrate that corrosion reactions at the Q235 carbon steel surface are effectively prevented by the BECP. Besides, the Q235 carbon steel presents E_{corr} of −1.0945 V and j_{corr} of 1.76 × 10^{-6} A·mm^{-2} under the potentiostat-

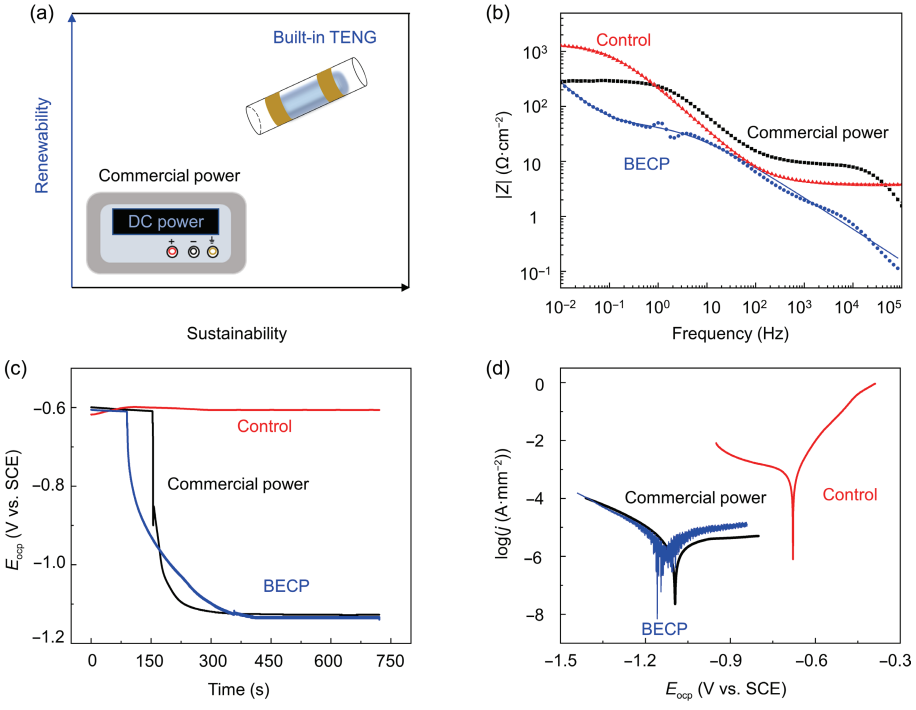

Figure 3 Electrochemical characterizations of Q235 carbon steel in 3.5 wt.% NaCl solution. (a) The schematic diagram shows our prototype's superiority over the traditional DC power. (b) Bode curves, (c) time-dependent variations of open-circuit potential, and (d) Tafel curves of Q235 carbon steel protected by our BECP at the operation frequency of 0.8 Hz, 5 V of a DC commercial potentiostat, and without any protection.

powered cathodic protection (5 V). In this condition, the Q235 carbon steel exhibits similar electrochemical behaviors to samples protected by BECP, which is verified by the close self-corrosion potential and self-corrosion current density. Therefore, the proposed BECP is suitable to replace commercial potentiostat-powered cathodic protection and exhibits great potential for turning marine energy into sustainable engineering electricity for metal material protection.

The above electrochemical measurements demonstrate the feasibility of cathodic protection, and we further carried out the intuitive anticorrosion application in simulated seawater. Here, a Q235 carbon steel plate with an area of 1 cm^2 was immersed in 3.5 wt.% NaCl solution and was connected directly to the negative terminal of the rectifier. To form a completely closed-circuit loop, we linked the positive terminal to a Pt electrode, which could be replaced by a carbon electrode or other inert electrodes. In contrast, control groups powered by a nonrenewable electricity source and without any protection were also performed.

To intuitively demonstrate effective protection, we mapped the size of corrosion pitting on the Q235 carbon steel surface and the accumulation of corrosion products in corrosive solution at each scheduled time plot. Generally, severe metal corrosion can be reflected by the occurrence of corrosion pitting and accumulation of corrosion products. For carbon steel without any protection, as presented in Fig. 4, the number of corrosion pitting dramatically increases, along with their sizes expanding to cover the entire surface. Simultaneously, the immersion solution turns into turbid for the corrosion products accumulation of aqueous Fe^{3+} ions and solid sludge. In contrast, current injection by our built-in TENG array provides additional electrons to the cathode surface and inhibits the competitive reaction of corrosion with chloride ions, water, and oxygen molecules. Benefitting from this, there is no apparent corrosion pitting on the carbon steel surface, and no prominent leaching of Fe^{3+} ions into the solution within 8 h as protected by the BECP, which is basically equivalent to the effect powered by a 5 V constant potential. With the immersion time lasting 22 h, there is still no appearance of corrosion pits on the Q235 steel surface and no accumulated corrosion products in the immersion solution. Therefore, our self-powered cathodic protection architecture is a valid alternative to other cathodic protection systems powered by nonrenewable electricity sources to promote green energy development and utilization simultaneously.

4 Conclusions

In summary, we proposed a BECP strategy that is capable of harnessing the low-frequency (mainly lower than 1.5 Hz) ocean wave energy for efficiently active anticorrosion. In particular, we leveraged an architecture with flexible water motion and high triboelectrification of water to the FEP surface to generate a prominent volumetric current density of 28.9 $mA{\cdot}m^{-3}$. Significantly, the volumetric current density is 5–20 times higher than other reported devices. We also successfully demonstrated that the proposed BECP is capable of protecting carbon steel free from corrosion without any external electricity input. Therefore, the BECP can be an alternative to the traditional active protection technology powered by nonrenewable electricity sources. Moreover, it can be easily applied on ships, buoys, and other offshore platforms to realize *in-situ* energy collection and cathodic protection to simultaneously promote green energy development and utilization.

Acknowledgements

We acknowledge the financial support from the National Natural Science Foundation of China (No. 51975502), the Research Grants Council of Hong Kong (Nos. SRFS2223-1S01, C1006-20W, 11213320, and 11219219), the Shenzhen Science and Technology Innovation Council (No. SGDX20201103093005028), the Innovation and Technology Commission of HongKong (Nos. GHP/021/19SZ and GHP/092/20GD), the Science and Technology Planning Project of Guangdong Province (No. 2021A0505110002), and the Tencent Foundation through the XPLORER PRIZE.

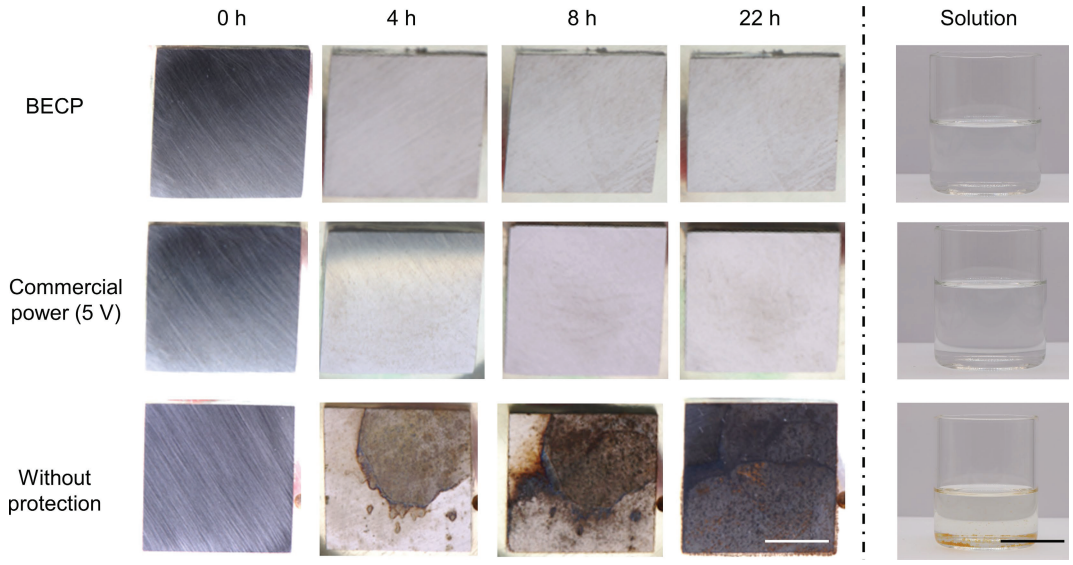

Figure 4 Corrosion comparison of the Q235 steel surface coupled with BECP, commercial power source, and without any protection. The left part shows the digital photographs of the surface evolution of Q235 carbon steels immersed in 3.5 wt.% NaCl solution for 0, 4, 8, and 22 h. The Q235 specimens were separated into three groups: The first group was protected by the BECP (operation frequency of 0.8 Hz), the second group was connected with the negative pole of 5 V of a constant-voltage potentiostat, and the third group was naturally corroded without any protection. The scale bar is 4 mm. The right part shows the corresponding salt solutions after 22 h of immersion, and the scale bar is 3 cm.

Electronic Supplementary Material: Supplementary material (the variation of the water–FEP contact interface corresponding to the different mechanical vibrating frequencies from 0.47 to 1.47 Hz, characterizations of the fabricated TENG, and electrochemical characterizations of the self-powered metal protection system) is available in the online version of this article at https://doi.org/10.1007/s12274-023-5623-0.

References

[1] Levitus, S. Boyer, T. P. *World Ocean Atlas 1994, Vol. 4, Temperature, NOAA*; U. S. Department of Commerce: Washington, 1994.

[2] Sabel, C. F.; Victor, D. G. Governing global problems under uncertainty: Making bottom–up climate policy work. *Clim. Change* **2017**, *144*, 15–27.

[3] Xia, D. H.; Deng, C. M.; Macdonald, D.; Jamali, S.; Mills, D.; Luo, J. L.; Strebl, M. G.; Amiri, M.; Jin, W. X.; Song, S. Z. et al. Electrochemical measurements used for assessment of corrosion and protection of metallic materials in the field: A critical review. *J. Mater. Sci. Technol.* **2022**, *112*, 151–183.

[4] Li, H. G.; Zhang, Y. B.; Li, C. H.; Zhou, Z. M.; Nie, X. L.; Chen, Y.; Cao, H. J.; Liu, B.; Zhang, N. Q.; Said, Z. et al. Cutting fluid corrosion inhibitors from inorganic to organic: Progress and applications. *Korean J. Chem. Eng.* **2022**, *39*, 1107–1134.

[5] Edalati, K.; Bachmaier, A.; Beloshenko, V. A.; Beygelzimer, Y.; Blank, V. D.; Botta, W. J.; Bryła, K.; Čížek, J.; Divinski, S.; Enikeev, N. A. et al. Nanomaterials by severe plastic deformation: Review of historical developments and recent advances. *Mater. Res. Lett.* **2022**, *10*, 163–256.

[6] Cao, Y. H.; Zheng, D. J.; Zhang, F.; Pan, J. S.; Lin, C. J. Layered double hydroxide (LDH) for multi-functionalized corrosion protection of metals: A review. *J. Mater. Sci. Technol.* **2022**, *102*, 232–263.

[7] Berdimurodov, E.; Verma, D. K.; Kholikov, A.; Akbarov, K.; Guo, L. The recent development of carbon dots as powerful green corrosion inhibitors: A prospective review. *J. Mol. Liq.* **2022**, *349*, 118124.

[8] Wang, Y. C.; Liu, B. Y.; Zhao, X. A.; Zhang, X. H.; Miao, Y. C.; Yang, N.; Yang, B.; Zhang, L. Q.; Kuang, W. J.; Li, J. et al. Turning a native or corroded Mg alloy surface into an anti-corrosion coating in excited CO_2. *Nat. Commun.* **2018**, *9*, 4058.

[9] Cui, M. M.; Wang, P. Y.; Wang, Z. K.; Wang, B. Mangrove inspired anti-corrosion coatings. *Coatings* **2019**, *9*, 725.

[10] Cui, M. M.; Wang, Z. K.; Wang, B. Survival strategies of mangrove (*Ceriops tagal* (*perr.*) *C. B. Rob*) and the inspired corrosion inhibitor. *Front. Mater.* **2022**, *9*, 879525.

[11] Raja, P. B.; Sethuraman, M. G. Natural products as corrosion inhibitor for metals in corrosive media—A review. *Mater. Lett.* **2008**, *62*, 113–116.

[12] Cui, M. M.; Njoku, D. I.; Li, B. W.; Yang, L. H.; Wang, Z. K.; Hou, B. R.; Li, Y. Corrosion protection of aluminium alloy 2024 through an epoxy coating embedded with smart microcapsules: The responses of smart microcapsules to corrosive entities. *Corros. Commun.* **2021**, *1*, 1–9.

[13] Njoku, D. I.; Cui, M. M.; Xiao, H. G.; Shang, B. H.; Li, Y. Understanding the anticorrosive protective mechanisms of modified epoxy coatings with improved barrier, active and self-healing functionalities: EIS and spectroscopic techniques. *Sci. Rep.* **2017**, *7*, 15597.

[14] Cao, X.; Jie, Y.; Wang, N.; Wang, Z. L. Triboelectric nanogenerators driven self-powered electrochemical processes for energy and environmental science. *Adv. Energy Mater.* **2016**, *6*, 1600665.

[15] Guo, W. X.; Li, X. Y.; Chen, M. X.; Xu, L.; Dong, L.; Cao, X.; Tang, W.; Zhu, J.; Lin, C. J.; Pan, C. F. et al. Electrochemical cathodic protection powered by triboelectric nanogenerator. *Adv. Funct. Mater.* **2014**, *24*, 6691–6699.

[16] Zhu, P. H.; Ullah, Z.; Zheng, S. R.; Yang, Z. R.; Yu, S. W.; Zhu, S. P.; Liu, L. W.; He, A. H.; Wang, C. G.; Li, Q. Ultrahigh current output from triboelectric nanogenerators based on UIO-66 materials for electrochemical cathodic protection. *Nano Energy* **2023**, *108*, 108195.

[17] Xu, C. G.; Liu, Y.; Liu, Y. P.; Zheng, Y. B.; Feng, Y. G.; Wang, B. Q.; Kong, X.; Zhang, X. L.; Wang, D. A. New inorganic coating-based triboelectric nanogenerators with anti-wear and self-healing properties for efficient wave energy harvesting. *Appl. Mater. Today* **2020**, *20*, 100645.

[18] Zhang, X. L.; Zheng, Y. B.; Wang, D. A.; Rahman, Z. U.; Zhou, F. Liquid–solid contact triboelectrification and its use in self-powered nanosensor for detecting organics in water. *Nano Energy* **2016**, *30*, 321–329.

[19] Sun, W. X.; Zheng, Y. B.; Li, T. H.; Feng, M.; Cui, S. W.; Liu, Y. P.; Chen, S. G.; Wang, D. A. Liquid–solid triboelectric nanogenerators array and its applications for wave energy harvesting and self-powered cathodic protection. *Energy* **2021**, *217*, 119388.

[20] Jeon, S. B.; Kim, D.; Seol, M. L.; Park, S. J.; Choi, Y. K. 3-Dimensional broadband energy harvester based on internal hydrodynamic oscillation with a package structure. *Nano Energy* **2015**, *17*, 82–90.

[21] Cui, S. W.; Zheng, Y. B.; Liang, J.; Wang, D. A. Triboelectrification based on double-layered polyaniline nanofibers for self-powered cathodic protection driven by wind. *Nano Res.* **2018**, *11*, 1873–1882.
[22] Cui, S. W.; Wang, J. P.; Mi, L. W.; Chen, K. Y.; Ai, W. Y.; Zhai, L. P.; Guan, X. Y.; Zheng, Y. B.; Wang, D. A. A new synergetic system based on triboelectric nanogenerator and corrosion inhibitor for enhanced anticorrosion performance. *Nano Energy* **2022**, *91*, 106696.
[23] Cui, S. W.; Zheng, Y. B.; Liang, J.; Wang, D. A. Conducting polymer PPy nanowire-based triboelectric nanogenerator and its application for self-powered electrochemical cathodic protection. *Chem. Sci.* **2016**, *7*, 6477–6483.
[24] Feng, Y. G.; Zheng, Y. B.; Rahman, Z. U.; Wang, D. A.; Zhou, F.; Liu, W. M. Paper-based triboelectric nanogenerators and their application in self-powered anticorrosion and antifouling. *J. Mater. Chem. A* **2016**, *4*, 18022–18030.
[25] Liu, Y. P.; Sun, W. X.; Li, T. H.; Wang, D. A. Hydrophobic MAO/FSG coating based TENG for self-healable energy harvesting and self-powered cathodic protection. *Sci. China:Technol. Sci.* **2022**, *65*, 726–734.
[26] Sun, W. X.; Wang, N. N.; Li, J. R.; Xu, S. W.; Song, L.; Liu, Y. P.; Wang, D. A. Humidity-resistant triboelectric nanogenerator and its applications in wind energy harvesting and self-powered cathodic protection. *Electrochim. Acta* **2021**, *391*, 138994.
[27] Han, J. J.; Liu, Y.; Feng, Y. W.; Jiang, T.; Wang, Z. L. Achieving a large driving force on triboelectric nanogenerator by wave-driven linkage mechanism for harvesting blue energy toward marine environment monitoring. *Adv. Energy Mater.* **2023**, *13*, 2203219.
[28] Liu, Y. P.; Sun, G. Y.; Liu, Y.; Sun, W. X.; Wang, D. A. Hydrophobic organic coating based water–solid TENG for water-flow energy collection and self-powered cathodic protection. *Front. Mater. Sci.* **2021**, *15*, 601–610.
[29] Zhong, Y. M.; Guo, Y. C.; Wei, X. X.; Rui, P. S.; Du, H. J.; Wang, P. H. Multi-cylinder-based hybridized electromagnetic-triboelectric nanogenerator harvesting multiple fluid energy for self-powered pipeline leakage monitoring and anticorrosion protection. *Nano Energy* **2021**, *89*, 106467.
[30] Feng, Y. W.; Han, J. J.; Xu, M. J.; Liang, X.; Jiang, T.; Li, H. X.; Wang, Z. L. Blue energy for green hydrogen fuel: A self-powered electrochemical conversion system driven by triboelectric nanogenerators. *Adv. Energy Mater.* **2022**, *12*, 2103143.
[31] Cao, B.; Wang, P. H.; Rui, P. S.; Wei, X. X.; Wang, Z. X.; Yang, Y. W.; Tu, X. B.; Chen, C.; Wang, Z. Z.; Yang, Z. Q. et al. Broadband and output-controllable triboelectric nanogenerator enabled by coupling swing-rotation switching mechanism with potential energy storage/release strategy for low-frequency mechanical energy harvesting. *Adv. Energy Mater.* **2022**, *12*, 2202627.
[32] Zhang, X. M.; Yang, Q. X.; Ji, P. Y.; Wu, Z. F.; Li, Q. Y.; Yang, H. K.; Li, X. C.; Zheng, G. C.; Xi, Y.; Wang, Z. L. Modeling of liquid–solid hydrodynamic water wave energy harvesting system based on triboelectric nanogenerator. *Nano Energy* **2022**, *99*, 107362.
[33] Cheng, P.; Guo, H. Y.; Wen, Z.; Zhang, C. L.; Yin, X.; Li, X. Y.; Liu, D.; Song, W. X.; Sun, X. H.; Wang, J. et al. Largely enhanced triboelectric nanogenerator for efficient harvesting of water wave energy by soft contacted structure. *Nano Energy* **2019**, *57*, 432–439.
[34] Wang, H. Y.; Zhu, Q. Y.; Ding, Z. Y.; Li, Z. L.; Zheng, H. W.; Fu, J. J.; Diao, C. L.; Zhang, X. N.; Tian, J. J.; Zi, Y. L. A fully-packaged ship-shaped hybrid nanogenerator for blue energy harvesting toward seawater self-desalination and self-powered positioning. *Nano Energy* **2019**, *57*, 616–624.
[35] Feng, Y. W.; Jiang, T.; Liang, X.; An, J.; Wang, Z. L. Cylindrical triboelectric nanogenerator based on swing structure for efficient harvesting of ultra-low-frequency water wave energy. *Appl. Phys. Rev.* **2020**, *7*, 021401.
[36] Zhu, H. R.; Tang, W.; Gao, C. Z.; Han, Y.; Li, T.; Cao, X.; Wang, Z. L. Self-powered metal surface anti-corrosion protection using energy harvested from rain drops and wind. *Nano Energy* **2015**, *14*, 193–200.
[37] Wu, H.; Mendel, N.; Van Den Ende, D.; Zhou, G. F.; Mugele, F. Energy harvesting from drops impacting onto charged surfaces. *Phys. Rev. Lett.* **2020**, *125*, 078301.
[38] Wang, L. L.; Song, Y. X.; Xu, W. H.; Li, W. B.; Jin, Y. K.; Gao, S. W.; Yang, S. Y.; Wu, C. Y.; Wang, S.; Wang, Z. K. Harvesting energy from high-frequency impinging water droplets by a droplet-based electricity generator. *EcoMat* **2021**, *3*, e12116.
[39] Wei, X. L.; Zhao, Z. H.; Zhang, C. G.; Yuan, W.; Wu, Z. Y.; Wang, J.; Wang, Z. L. All-weather droplet-based triboelectric nanogenerator for wave energy harvesting. *ACS Nano* **2021**, *15*, 13200–13208.
[40] Wang, Y.; Gao, S. W.; Xu, W. H.; Wang, Z. K. Nanogenerators with superwetting surfaces for harvesting water/liquid energy. *Adv. Funct. Mater.* **2020**, *30*, 1908252.
[41] Zhang, N.; Zhang, H. M.; Xu, W. H.; Gu, H. J.; Ye, S. M.; Zheng, H. X.; Song, Y. X.; Wang, Z. K.; Zhou, X. F. A droplet-based electricity generator with ultrahigh instantaneous output and short charging time. *Droplet* **2022**, *1*, 56–64.
[42] Jin, Y. K.; Wu, C. Y.; Sun, P. C.; Wang, M. M.; Cui, M. M.; Zhang, C.; Wang, Z. K. Electrification of water: From basics to applications. *Droplet* **2022**, *1*, 92–109.
[43] Toffoli, A.; Bitner-Gregersen, E. M. Types of ocean surface waves, wave classification. In *Encyclopedia of Maritime and Offshore Engineering*. Carlton, J.; Jukes, P.; Choo, Y. S., Eds.; John Wiley & Sons: New York, 2017; pp 1–8.
[44] Lee, U. J.; Jeong, W. M.; Cho, H. Y. Estimation and analysis of JONSWAP spectrum parameter using observed data around Korean coast. *J. Mar. Sci. Eng.* **2022**, *10*, 578.
[45] Jiang, D. Y.; Xu, M. Y.; Dong, M.; Guo, F.; Liu, X. H.; Chen, G. J.; Wang, Z. L. Water–solid triboelectric nanogenerators: An alternative means for harvesting hydropower. *Renewable Sustainable Energy Rev.* **2019**, *115*, 109366.
[46] Xu, W. H.; Zheng, H. X.; Liu, Y.; Zhou, X. F.; Zhang, C.; Song, Y. X.; Deng, X.; Leung, M.; Yang, Z. B.; Xu, R. X. et al. A droplet-based electricity generator with high instantaneous power density. *Nature* **2020**, *578*, 392–396.
[47] Xu, W. H.; Song, Y. X.; Xu, R. X.; Wang, Z. K. Electrohydrodynamic and hydroelectric effects at the water–solid interface: From fundamentals to applications. *Adv. Mater. Interfaces* **2021**, *8*, 2000670.
[48] Basset, P.; Beeby, S. P.; Bowen, C.; Chew, Z. J.; Delbani, A.; Dharmasena, R. D. I. G.; Dudem, B.; Fan, F. R.; Galayko, D.; Guo, H. Y. et al. Roadmap on nanogenerators and piezotronics. *APL Mater.* **2022**, *10*, 109201.
[49] Zheng, H. X.; Wu, H.; Yi, Z. R.; Song, Y. X.; Xu, W. H.; Yan, X. T.; Zhou, X. F.; Wang, S.; Wang, Z. K. Remote-controlled droplet chains-based electricity generators. *Adv. Energy Mater.*, in press, https://doi/org/10.1002/aenm.202203825.
[50] Zhao, X. J.; Kuang, S. Y.; Wang, Z. L.; Zhu, G. Highly adaptive solid–liquid interfacing triboelectric nanogenerator for harvesting diverse water wave energy. *ACS Nano* **2018**, *12*, 4280–4285.
[51] Zhang, N.; Gu, H. J.; Zheng, H. X.; Ye, S. M.; Kang, L.; Huang, C.; Lu, K. Y.; Xu, W. H.; Miao, Q. Q.; Wang, Z. K. et al. Boosting the output performance of volume effect electricity generator (VEEG) with water column. *Nano Energy* **2020**, *73*, 104748.
[52] Von Baeckmann, W.; Schwenk, W.; Prinz, W. *Handbook of Cathodic Corrosion Protection*; Gulf Professional Publishing: Houston, 1997.